# Value of monoenergetic dual-energy CT (DECT) for artefact reduction from metallic orthopedic implants in post-mortem studies

Filograna, Laura ; Magarelli, Nicola ; Leone, Antonio ; Guggenberger, Roman ; Winklhofer, Sebastian ; Thali, Michael John ; Bonomo, Lorenzo

Abstract: OBJECTIVES: The aim of this ex vivo study was to assess the performance of monoenergetic dual-energy CT (DECT) reconstructions to reduce metal artefacts in bodies with orthopedic devices in comparison with standard single-energy CT (SECT) examinations in forensic imaging. Forensic and clinical impacts of this study are also discussed. MATERIALS AND METHODS: Thirty metallic implants in 20 consecutive cadavers with metallic implants underwent both SECT and DECT with a clinically suitable scanning protocol. Extrapolated monoenergetic DECT images at 64, 69, 88, 105, 120, and 130 keV and individually adjusted monoenergy for optimized image quality (OPTkeV) were generated. Image quality of the seven monoenergetic images and of the corresponding SECT image was assessed qualitatively and quantitatively by visual rating and measurements of attenuation changes induced by streak artefact. RESULTS: Qualitative and quantitative analyses showed statistically significant differences between monoenergetic DECT extrapolated images and SECT, with improvements in diagnostic assessment in monoenergetic DECT at higher monoenergies. The mean value of OPTkeV was 137.6 ± 4.9 with a range of 130 to 148 keV. CONCLUSIONS: This study demonstrates that monoenergetic DECT images extrapolated at high energy levels significantly reduce metallic artefacts from orthopedic implants and improve image quality compared to SECT examination in forensic imaging.

DOI: https://doi.org/10.1007/s00256-015-2155-z

Skeletal Radiol (2015) 44:1287–1294
DOI 10.1007/s00256-015-2155-z

SCIENTIFIC ARTICLE

# Value of monoenergetic dual-energy CT (DECT) for artefact reduction from metallic orthopedic implants in post-mortem studies

**Laura Filograna [1,3] · Nicola Magarelli [3] · Antonio Leone [3] · Roman Guggenberger [2] · Sebastian Winklhofer [2] · Michael John Thali [1] · Lorenzo Bonomo [3]**

Received: 14 January 2015 / Revised: 10 April 2015 / Accepted: 16 April 2015 / Published online: 12 May 2015


**Abstract**
*Objectives* The aim of this ex vivo study was to assess the performance of monoenergetic dual-energy CT (DECT) reconstructions to reduce metal artefacts in bodies with orthopedic devices in comparison with standard single-energy CT (SECT) examinations in forensic imaging. Forensic and clinical impacts of this study are also discussed.
*Materials and methods* Thirty metallic implants in 20 consecutive cadavers with metallic implants underwent both SECT and DECT with a clinically suitable scanning protocol. Extrapolated monoenergetic DECT images at 64, 69, 88, 105, 120, and 130 keV and individually adjusted monoenergy for optimized image quality (OPTkeV) were generated. Image quality of the seven monoenergetic images and of the corresponding SECT image was assessed qualitatively and quantitatively by visual rating and measurements of attenuation changes induced by streak artefact.
*Results* Qualitative and quantitative analyses showed statistically significant differences between monoenergetic DECT extrapolated images and SECT, with improvements in diagnostic assessment in monoenergetic DECT at higher monoenergies. The mean value of OPTkeV was 137.6±4.9 with a range of 130 to 148 keV.
*Conclusions* This study demonstrates that monoenergetic DECT images extrapolated at high energy levels significantly reduce metallic artefacts from orthopedic implants and improve image quality compared to SECT examination in forensic imaging.

**Keywords** Dual-energy computed tomography · Monoenergetic extrapolation · Metallic artefact reduction · Forensic imaging · Post-mortem CT

## Introduction

Imaging techniques have been widely introduced in forensic investigations, with post-mortem computed tomography (PMCT) and post-mortem magnetic resonance (PMMR) being the methods of choice [1–6]. One of the most important advantages of PMCT against PMMR examinations is the optimal visualization of skeletal structures with the possibility of 2D and 3D reconstructions that offer a panoramic view of isolated bones and of the entire skeleton. Performing whole-body PMCT is considered mandatory in cases of fatal trauma or of suspected orthopedic malpractice [7–10]. Moreover, the comparison of ante-mortem and post-mortem CT data sets has a role in personal identification [11].

Nevertheless, PMCT diagnostic capabilities are significantly limited by metal artefacts originating from metal objects, such as orthopedic implants [12]. In the presence of metal objects, the artefacts from quantum noise, beam hardening, and scattered radiation [13–15] can markedly impair proper visualization of the implant itself, the implant–bone interface, the bone, and the surrounding soft tissue.

Various methods have been proposed for reducing metal artefacts and improving image quality in CT examinations,

✉ Laura Filograna
laura.filograna@rm.unicatt.it

1 Department of Forensic Medicine and Imaging, Institute of Forensic Medicine, University of Zurich, Winterthurerstrasse 190/52, 8057 Zurich, Switzerland

2 Institute of Diagnostic and Interventional Radiology, University Hospital Zurich, Raemistrasse 100, 8091 Zurich, Switzerland

3 Present address: Department of Radiological Sciences, Catholic University of Rome, School of Medicine, University Hospital "A. Gemelli", Largo A. Gemelli 8, 00168 Rome, Italy

and these are based mainly on adjustments of CT acquisition or post-processing algorithms [12, 16–26].

In recent years, dual-energy CT (DECT) has been introduced in clinical musculoskeletal imaging as a viable method for reducing metal artefacts by means of both acquisition and reconstruction capabilities [27].

In DECT, two CT datasets are acquired with different X-ray spectra by switching the voltage of one X-ray tube or by running two tubes at different voltages. Several technical approaches have been proposed that include sequential acquisition, rapid voltage switching, dual-source CT (DSCT), layer detector, quantum-counting detector. The two obtained data sets can be used to extrapolate monoenergetic image reconstructions, related to a specific energy level [27]. Extrapolating images at specifically higher monoenergetic levels has been proven to better reduce metallic artefacts than lower monoenergetic levels [27].

Image quality for identification purposes can be improved in patients with extensive dental restoration [28]. Although promising, monoenergetic DECT has only scarcely been used in the forensic field.

In this ex vivo study, for the first time monoenergetic DECT reconstructions of skeletal segments with different metallic orthopedic devices were compared with real standard single-energy CT (SECT) images performed on the same post-mortem study population with equal, clinically suitable, radiation doses. The aim of the study was to investigate the ability of DECT techniques to reduce metal artefacts in post-mortem cases. Forensic and clinical impacts of this study are discussed.

## Materials and methods

### Study population

This prospective study was approved by both our institutional review board and the responsible justice department.

A total of 30 internal metallic implants in 20 consecutive cadavers (nine males and 11 females, mean age 74±15 years, range, 43–92 years) that were delivered to our institute for forensic investigation, including PMCT examination, were included into this study between February and May 2014 (Table 1). Inclusion criterion was the evidence of prior implanted metal devices and exclusion criterion was the presence of major alterations of the soft tissues near the implant (for example those due to putrefaction, laceration, infection).

### CT data acquisition

All examinations were performed on a dual-source CT (Somatom Definition Flash, Siemens Medical, Forchheim, Germany).

**Table 1** Types of metal devices examined in this study

| Metal device number | Type of metallic device |
|---|---|
| 1. | Tibial screw |
| 2. | Hip prosthesis |
| 3. | Hip prosthesis |
| 4. | Tibial plate and screws |
| 5. | Hip prosthesis |
| 6. | Humeral head screw |
| 7. | Humeral plate and screws |
| 8. | Tibial screw |
| 9. | Tibial plate and screws |
| 10. | Hip prosthesis |
| 11. | Gamma nail osteosynthesis |
| 12. | Knee prosthesis |
| 13. | Knee prosthesis |
| 14. | Shoulder prosthesis |
| 15. | Gamma nail osteosynthesis |
| 16. | Gamma nail osteosynthesis |
| 17. | Knee prosthesis |
| 18. | Pedicle screws after spondylodesis |
| 19. | Tibial screws |
| 20. | Fibular plate and screws |
| 21. | Femoral intramedullary nail |
| 22. | Femoral intramedullary nail |
| 23. | Patellar screw |
| 24. | Glenoid screws |
| 25. | Hip prosthesis |
| 26. | Femoral plate and screws |
| 27. | Hip prosthesis |
| 28. | Hip prosthesis |
| 29. | Humeral plate and screws |
| 30. | Gamma nail osteosynthesis |

In both single-energy CT (SECT) and dual-energy CT (DECT) scans, the tube currents were manually selected in each examination to keep the volume CT dose index fixed at 20.0 mGy, being similar to that applied in clinical CT scans of the skeletal system. Actually, the dose of 20.0 mGy for extremities is slightly higher than that used in the routine clinical practice for this anatomical region. Nevertheless, in this study, it was chosen to use the same dose for each CT examination and body district in order to obtain more homogeneous and comparable images. Moreover, the low radiosensitivity of the extremities should be taken into account. For SECT acquisitions, the following parameters were chosen: slice acquisition

32×1.2 mm, pitch 0.5, rotation time 0.5 s, tube voltage 120 kVp, tube current-time 297 mAs/rotation. DECT scans were performed with the following parameters: slice acquisition 2× 32×0.6 mm, pitch 0.5, rotation time 0.5 s, and a tube voltage pair of 100 and 140 kVp for tube A and tube B, respectively. A tin filter was applied to tube B for better energy spectrum separation [29]. Tube current-time products for DECT were 211 mAs/rotation for both tubes.

## CT image reconstruction and analysis

SECT and DECT datasets were reconstructed with a slice thickness of 1.5 mm and an increment of 1 mm using a fixed field of view (FoV) of 200 mm (image matrix 512×512), and two convolution kernels, B60f and D30f, to optimize the protocol for the assessment of bony structures and soft tissue, respectively.

Post-processing of DECT data sets was performed using commercially available software (syngo, software VA31, monoenergetic application) installed on a Leonardo workstation (Siemens HealthCare, Forchheim, Germany). This software is able to extract the monoenergetic images at arbitrary photon energies ranging from 40 to 190 keV. Then, DECT reconstructions performed with the sharpest kernel were used to obtain six monoenergetic data sets at 64, 69, 88, 105, 120, and 130 keV and at the optimized keV value (OPTkeV), which was manually selected from a possible range of monoenergies from 40 to 190 keV (Figs. 1 and 2). In particular, the OPTkeV was chosen such that images showed the fewest streak artefacts and best image quality. The three energy levels (64, 69, and 88 keV) were selected because they matched the mean energies of the respective standard 120-kVp, 140-kVp, and tin-filtered 140-kVp spectra. The monoenergy values of 105, 120, and 130 keV were chosen based on previous studies on metallic implants in various body parts [30–32].

For all imaging analyses, standard bone window settings (width 1900 Hounsfield Units - HU, center 500 HU) were used by default.

First, from the SECT dataset, one single slice with the thickest area of the metallic implant and the most pronounced streak artefacts was selected in axial plane images.

Corresponding axial images of monoenergetic DECT datasets at 64, 69, 88, 105, 120, and 130 keV and at OPT keV were identified in the same z-position.

Then, two radiologists with 3 and 18 years of experience in musculoskeletal imaging (L.F. and N.M., respectively), and 12 years of experience in forensic radiology (L.F.), and who were blinded to each other's qualitative assessments, assessed the artefacts in these seven selected images and the corresponding SECT image. For the qualitative analysis, the two observers rated the degree of artefacts and overall image quality using a four-point Likert scale: (1) absence of artefacts and excellent image quality with full diagnostic interpretability; (2) minor artefacts and good image quality with confident diagnostic interpretability; (3) significant artefacts and limited image quality with impaired diagnostic interpretability, but still suitable for diagnostic purposes; (4) massive streak artefacts and markedly reduced image quality, with abolished diagnostic interpretability.

Then, to perform a quantitative analysis of the artefacts, the density (Hounsfield Unit value – HU) of the most marked streak artefact in the one SECT image and the seven monoenergetic DECT reconstructions was calculated. The measurement was performed by using a circular region of interest (ROI), of approximately the same size in both SECT

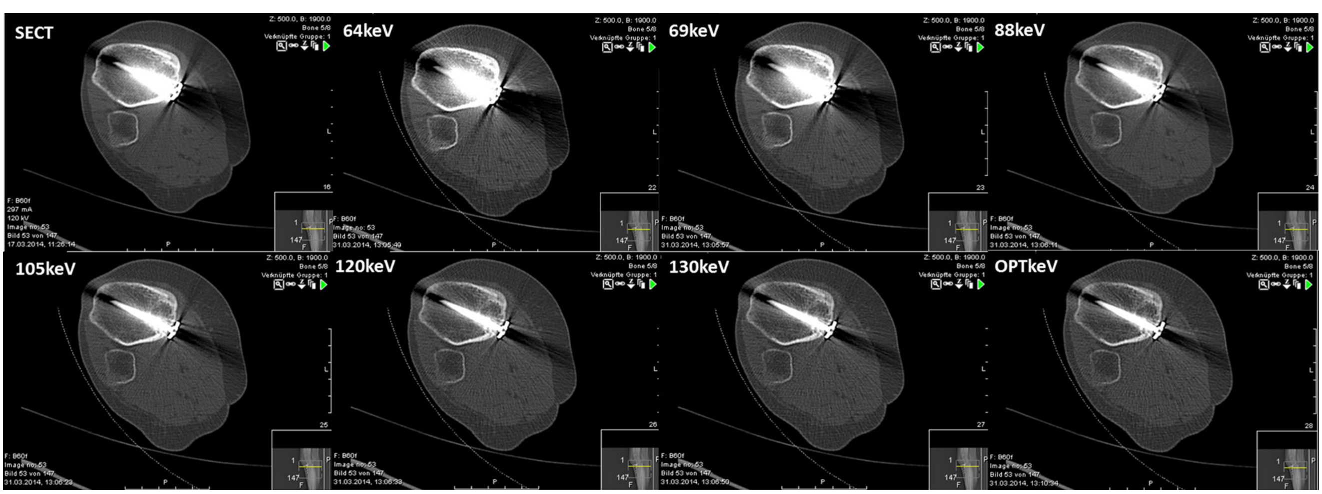


**Fig. 1** Examples of images from a patient with tibial plate and screws (case 9). Images from SECT scan and DECT extrapolated datasets at 64, 69, 88, 105, 120, 130, and optimized keV (OPTkeV, corresponding to 136 keV) are shown at an identical axial level and at the same standard bone window (width 1900 HU, center 500 HU). Note that the image quality improves at higher DECT monoenergies compared with the SECT image with the possibility of differentiating the bone–metal interface at 120 and 130 keV, and at OPTkeV. A better reduction of artefacts can be recognized in the SECT image with respect to the corresponding monoenergetic DECT image (i.e., extrapolated at 64 keV)


**Fig. 2** Representative images in a patient with posterior spinal fusion implants of the lumbar spine (case 18). Images from SECT scan and DECT extrapolated datasets at 64, 69, 88, 105, 120, 130, and optimized keV (OPTkeV, corresponding to 138 keV) are shown at an identical axial level and at the same standard bone window (width 1900 HU, center 500 HU). SECT and monoenergetic DECT extrapolations at 64 and 69 keV show the worse image quality with marked streak artefacts. Decreasing streak artefacts are seen at increasing extrapolated monoenergies from DECT data at 88, 105, 120, and 130 keV, and at OPTkeV with the possibility of correctly visualizing the bone–metal interfaces

and DECT images, that was placed within the hypodense streak area adjacent to the metallic implant, and far from the edge of the artefacts in order to avoid spurious results. In addition, a reference density measurement was obtained by placing a ROI in an area containing fat and muscle located far from the hypodense streak of artefact and thus not affected by the artefact. The artefact intensity was calculated by subtracting the streak density from the reference density. The quantitative analysis was performed by a single observer (L.F.), who repeated the measurements after 1 month to assess intra-observer variability.

### Statistical analysis

Quantitative variables are expressed as mean±standard deviation and categorical variables as frequencies or percentages.

Inter-reader agreements of qualitative parameters (i.e., degree of artefacts and overall image quality) were analyzed with weighted kappa statistics. According to Landis and Koch, kappa values of 0.61–0.80 were interpreted as substantial, and 0.81–1.00 as excellent agreement [33].

To compare the image quality between the different monoenergetic images (64, 69, 88, 105, 120, and 130 keV and OPTkeV) and the SECT images the Mantel–Haenszel $\chi 2$-test was carried out. In addition, Cramer's V correlation coefficient was used to analyze associations between image quality with the different keV (DECT) and kVp (SECT) settings.

Pairwise comparisons of the qualitative assessment of artefact scores and CT attenuation values of artefacts between the datasets (64, 69, 88, 105, 120, and 130 keV and OPTkeV) were carried out using Wilcoxon signed-rank test.

Intra-reader agreement of quantitative analyses of CT numbers of artefacts and reference tissue were analyzed with intraclass correlation coefficients (ICC). ICC values were interpreted as follows: poor (ICC<0.69), fair (ICC=0.70–0.79), good (ICC=0.80–0.89), or high (ICC>0.90) [34].

Related-samples Friedman's analyses were used to compare quantitative CT numbers of artefacts and reference tissues between the different datasets (64, 69, 88, 105, 120, and 130 keV, OPTkeV, and SECT).

A two-tailed $p$ value<0.05 was considered statistically significant. Statistical analyses were performed using commercially available software (IBM SPSS Statistics, Version 21.0. Armonk, NY: IBM Corp.

## Results

### Qualitative analysis

The inter-reader agreement for qualitative assessment of degree of artefacts and overall image quality with the four-point Likert scale was excellent (0.933, $p$<0.001). In both readers (R1 and R2), the median image quality score was significantly ($p$<0.001 for both) different between SECT and monoenergetic DECT images at 64, 69, 88, 105, 120, and 130 keV, and at OPTkeV. The median image quality score was the same in R1 and R2 for 64 keV (4.0), 69 keV (4.0), 88 keV (3.0), 105 keV (2.0), 130 keV (1.0), SECT (3.0) and OPTkeV (1.0), and was only different in 120 keV (R1: 1.5 and R2: 1.0). The image quality improved at higher DECT monoenergies compared with the SECT images (R1: V=0.526, R2 V=0.536; $p$<0.001 for both). In pairwise comparisons, OPTkeV data sets of both readers showed a significantly lower (i.e., better image quality) median image quality score compared with data sets of 64, 69, 88, 105, and 120 keV and SECT ($p<0.05$ for both). No significant difference was found between OPTkeV and 130 keV ($p=0.317$ for both). In pairwise comparisons, SECT data sets of both readers showed a significantly lower median image quality score compared with data sets of 64 and 69 keV ($p<0.001$ for both). No significant difference was found between SECT and 88 keV (R1: $p=0.180$; R2: $p=0.317$). SECT data sets of both readers showed a significantly higher median image quality score (i.e., worse image quality) compared with data sets of 105, 120, and 130 keV and OPTkeV ($p<0.001$ for both).

### Quantitative analysis

For intra-reader agreement analysis, CT number measurements were significantly correlated ($p<0.001$) with ICCs demonstrating excellent agreement (ICC=0.977). Hence, mean measurements were taken for further calculations. The results of the quantitative analysis are shown schematically in Fig. 3.

CT numbers of artefacts were significantly ($p<0.001$) different between all data sets (SECT, monoenergetic images at 64, 69, 88, 105, 120, and 130 keV, and at OPTkeV). In contrast, CT numbers of the reference tissue did not differ between the datasets ($p=0.851$). The mean value of OPTkeV was 137.6±4.9 with a range of 130–148 keV.

The mean HU attenuation values of streak artefacts were −608±274, −535±279, −312±228, −207±220, −153±216, −126±214, −327±240 and −104±203 for 64, 69, 88, 105, 120, and 130 keV, SECT, and OPTkeV, respectively.

Pairwise comparisons demonstrated significant ($p<0.001$, each) higher CT numbers (i.e., reduction of streak artefact density) in OPTkeV compared to all other datasets (64, 69, 88, 105, 120, and 130 keV and SECT).

Pairwise comparisons demonstrated significantly higher CT numbers in SECT compared to 64 and 69 keV but significantly lower CT numbers in SECT compared to 105, 120, and 130 keV and OPTkeV.

No statistical significant differences were found between 88 keV and SECT images ($p=0.318$)

## Discussion

Even if we consider the ex-vivo study by Guggenberger [35], who investigated the optimal monoenergetic DECT settings for artefact reduction of posterior spinal fusion implants in phantoms, this is the first study on cadavers in this field of investigation. As a consequence, in this ex vivo study, for the first time for different skeletal segments and metallic orthopedic devices, a real comparison between SECT and extrapolated monoenergetic DECT datasets could be performed.

In fact, in similar previous clinical studies [30–32], the performance of DECT technology in reducing metallic artefacts was not tested in comparison with real SECT, for

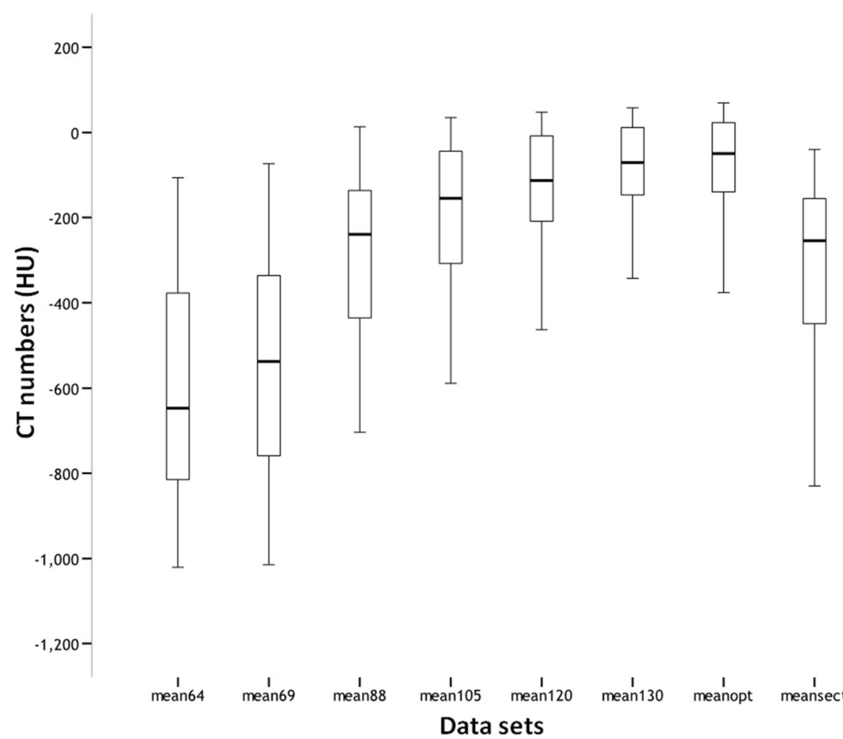


**Fig. 3** Box plots show the CT numbers of streak artefacts with respect to datasets of SECT, monoenergetic extrapolation of DECT data at 64, 69, 88, 105, 120, and 130 keV and optimized keV (OPTkeV). CT numbers of artefacts were significantly ($p<0.01$) different between datasets, and demonstrated the best performances at OPTkeV. SECT showed significantly higher CT numbers compared with 64 and 69 keV, but significantly lower CT numbers in SECT compared with 105, 120, and 130 keV, and with OPTkeV

obvious reasons related to radioprotection. More specifically, SECT datasets for comparison were obtained by using DECT spectra at 64, 69, and 88 keV, (simulated 120 kVp, 140 kVp, and tin filtered 140-kVp SECT datasets, respectively), or by scoring the unprocessed DECT images obtained at 140 kVp or by using SECT 120-kVp averaged images from both tubes.

As previously demonstrated in a clinical setting, this work confirms the superiority of monoenergetic reconstructions extracted from DECT data sets over SECT for metal artefact reduction in post-mortem scans of individuals with orthopedic hardware [27].

DECT has already been proposed as a useful technique for increasing the interpretability of clinical examinations by reducing metallic artefacts. In post-procedural imaging, an optimal display of bones, implants and bone–implant interfaces is crucial for early detection of complications following metallic device placements (for example, implant fracture, loosening, faults, and infections) [14, 15, 36].

Bamberg compared the performance of DECT monoenergetic images to extrapolated standard 120- and 140-kVp spectra and filtered 140-kVp spectrum in 31 patients with metallic implants of different types and vendors [30]. The study proved that monoenergetic DECT reconstructions are able to improve image quality by 49 % and can enhance the diagnostic value by approximately 44 % [30]. Zhou et al. analyzed 47 patients who underwent osteosynthesis implantation for fracture fixation with the goal of reducing metallic artefacts by optimization of the photo-energy settings. They recommended an overall setting of 130 keV [31]. Similarly, Meinel et al. performed a study on a hip phantom and 22 patients with various metallic orthopedic implants to define an optimized image acquisition protocol for reducing artefacts [32]. They found that the optimal parameters for improving image quality are: Sn 140/100 kVp with a current tube ratio 3:1, a collimation of 32×0.6 mm and extrapolated energies of 105 to 120 keV in all types of metal implants [32]. Moreover, Guggenberger et al. in an ex-vivo study on phantoms compared the performances of DECT monoenergetic reconstructions with equivalent standard SECT images in reducing metallic artefact from posterior spinal fusion implants of various vendors and spine levels [35]. Their study showed that DECT improves image quality and reduces metallic artefacts compared to SECT [35].

Furthermore, in forensics, particularly in traumatic cases of death, it would be desirable to correctly visualize the same structures to identify first the presence of fractures and surrounding soft-tissue injuries and then to analyze the pattern of these injuries, particularly of the fractures, which is fundamental for conducting forensic reconstruction of the dynamics of the fatal event [7–10]. The reduction of metallic artefact from orthopedic devices should improve the identification process in the deceased, similar to that proposed by Stolzmann et al. regarding artefacts from dental restorations [28]. Furthermore, in cases of suspected orthopedic malpractice, the forensic pathologist would benefit from information about the position of an orthopedic implant and its relationship with the nearby soft tissues and vessels for making forensic conclusions.

In the reported post-mortem study, and in line with clinical findings, both qualitative and quantitative analyses showed significant differences between extrapolated monoenergetic DECT and SECT images, with a significant improvement in the diagnostic assessment in monoenergetic DECT at higher monoenergies.

The mean value of OPTkeV was 137.6±4.9 with a range of 130–148KeV. This value was greater than that found in some of the previous clinical studies on this issue, which investigated various orthopedic metallic implants [30–32]. In particular, the OPTkeV value was 105 keV (range, 95–150 keV) for Bumgerg [30], 113 keV (range, 100–130 keV) for Meinel [32] and 130 keV for Zhou [31]. These discrepancies might be explained by the differences in implant type (material composition and geometry) and body region, and by the limited sample size.

In addition, although quantitatively the OPTkeV provided the highest reduction of artefacts in all cases, no statistically relevant differences in image quality were observed between OPTkeV and 130 keV extrapolated images ($p$=0.317 for both). This means that an OPTkeV in the range 130–148 keV is able to provide images with quantitatively fewer streak artefacts than monoenergetic reconstructions at 130 keV, but almost the same image quality can be obtained at 130 keV and OPTkeV from 130 to 148 keV. Beyond this threshold, it is assumed that the tissue contrast of bones and the nearby tissues would be too impaired to provide high-quality diagnostic images. Further studies in a larger cohort with metallic devices of different composition and geometry may enhance the standardization of OPTkeV settings. Thus, we suggest the adjustment of the extrapolated photon energy to obtain the optimal diagnostic quality for each individual subject.

In addition, the results of this study prompt further comments.

Monoenergetic images at 64 keV (simulated 120 kVp SECT) were included in the evaluations of the present study and compared with real standard 120-kVp SECT images. Both the qualitative and quantitative analysis of artefacts gave results that were significantly different between 120-kVp SECT and simulated 120 kVp (i.e., monoenergetic DECT images at 64 keV), with the former showing better performance in terms of metal artefact reduction. This result suggests some caution in considering the SECT images and the corresponding simulated SECT obtained from DECT as completely equal during studies on the performance of DECT technologies. This is simply explained by the fact that a virtual mono-energetic image at 64 keV is not the best way to simulate a true poly-energetic SECT 120-kVp image.

This work has some limitations. First, as mentioned above, there is a certain paucity and heterogeneity of skeletal segments and metallic devices analyzed. Differences in optimal settings may vary depending on these factors. Our data were obtained in ex vivo settings. However, post-mortem studies in cadavers are the best way to simulate in vivo conditions. Nevertheless, we agree with Guggenberger et al. [35] who assumed that the origin of CT artefacts is largely hardware-dependent and not related to the in vivo or ex vivo conditions. Secondly, the impact of metal artefact reduction by DECT techniques on the results of forensic investigation was not investigated. We encountered too few cases with fractured bones in proximity to the implant and no single case where PMCT was performed for identification purposes through the comparison of ante- and post-mortem images of orthopedic implants. The limited access to DECT technologies for forensic purposes undoubtedly limits the impact of these results in routine forensic practice.

In conclusion, this study demonstrates that, as well as in clinical settings, monoenergetic DECT reconstructions can effectively and significantly reduce metal artefacts due to metal orthopedic implants and improve image quality in PMCT examinations. At the same clinically suitable radiation dose of 20 mGy, high monoenergetic levels ranging from 130 to 148 keV have been proved to provide a better image quality with respect to the corresponding SECT examinations. The improvements in image quality might be reflected in an added diagnostic value in forensic investigations on trauma or orthopedic malpractice cases.

**Acknowledgments** The authors would like to thank Tim Finkenstaedt, MD, radiologist at the Institute of Diagnostic and Interventional Radiology, University Hospital Zurich, for the assistance in conducting statistical analysis, and Dominic Gascho, radiology technician at the Department of Forensic Medicine and Imaging, Institute of Forensic Medicine, University of Zurich, for the experienced assistance and support in performing PMCT scans.

**Conflict of interest** The authors declare that they have no conflicts of interest.

## References

1. Thali MJ, Yen K, Schweitzer W, et al. Virtopsy, a new imaging horizon in forensic pathology: virtual autopsy by postmortem multislice computed tomography (MSCT) and magnetic resonance imaging (MRI)—a feasibility study. J Forensic Sci. 2003;48:1–18.
2. Kahana T, Hiss J. Forensic radiology. Br J Radiol. 1999;72:129–33.
3. Wallace SK, Cohen WA, Stern EJ, Reay DT. Judicial hanging: postmortem radiographic, CT, and MR imaging features with autopsy confirmation. Radiology. 1994;193:263–7.
4. Poulsen K, Simonsen J. Computed tomography in connection with medico-legal autopsies. Forensic Sci Int. 2007;171:190–7.
5. Hayakawa M, Yamamoto S, Motani H, Yajima D, Sato Y, Iwase H. Does imaging technology overcome problems of conventional postmortem examination. Int J Legal Med. 2006;120:24–6.
6. O'Donnell C, Woodford N. Post-mortem radiology—a new subspeciality? Clin Radiol. 2008;63:1189–94.
7. Shiotani S, Shiigai M, Ueno Y, et al. Postmortem computed tomography findings as evidence of traffic accident-related fatal injury. Radiat Med. 2008;26:253–60.
8. Sochor MR, Trowbridge MJ, Boscak A, Maino JC, Maio RF. Postmortem computed tomography as an adjunct to autopsy for analyzing fatal motor vehicle crash injuries: results of a pilot study. J Trauma. 2008;65:659–65.
9. Leth PM, Ibsen M. Abbreviated injury scale scoring in traffic fatalities: comparison of computerized tomography and autopsy. J Trauma. 2010;68:1413–6.
10. Scholing M, Saltzherr TP, Fung Kon Jin P, et al. The value of postmortem computed tomography as an alternative for autopsy in trauma victims: a systematic review. Eur Radiol. 2009;19:2333–41.
11. Thali MJ, Markwalder T, Jackowski C, Sonnenschein M, Dirnhofer R. Dental CT imaging as a screening tool for dental profiling: advantages and limitations. J Forensic Sci. 2006;51:113–9.
12. Lee MJ, Kim S, Lee SA, et al. Overcoming artifacts from metallic orthopedic implants at high-field-strength MR imaging and multidetector CT. Radiographics. 2007;27:791–803.
13. Watzke O, Kalender WA. A pragmatic approach to metal artifact reduction in CT: merging of metal artifact reduced images. Eur Radiol. 2004;14:849–56.
14. Barrett JF, Keat N. Artifacts in CT: recognition and avoidance. Radiographics. 2004;24:1679–91.
15. Haramati N, Staron RB, Mazel-Sperling K, et al. CT scans through metal scanning technique versus hardware composition. Comput Med Imaging Graph. 1994;18:429–34.
16. Douglas-Akinwande AC, Buckwalter KA, Rydberg J, Rankin JL, Choplin RH. Multichannel CT: evaluating the spine in postoperative patients with orthopedic hardware. Radiographics. 2006;26:S97–110.
17. Buckwalter KA, Parr JA, Choplin RH, Capello WN. Multichannel CT imaging of orthopedic hardware and implants. Semin Musculoskelet Radiol. 2006;10:86–97.
18. Kachelriess M, Watzke O, Kalender WA. Generalized multidimensional adaptive filtering for conventional and spiral single slice, multi-slice, and cone-beam CT. Med Phys. 2001;28:475–90.
19. Veldkamp WJ, Joemai RM, van der Molen AJ, Geleijns J. Development and validation of segmentation and interpolation techniques in sinograms for metal artifact suppression in CT. Med Phys. 2010;37:620–8.
20. Mahnken AH, Raupach R, Wildberger JE, et al. A new algorithm for metal artifact reduction in computed tomography: in vitro and in vivo evaluation after total hip replacement. Investig Radiol. 2003;38:769–75.
21. Bal M, Spies L. Metal artifact reduction in CT using tissue-class modeling and adaptive prefiltering. Med Phys. 2006;33:2852–9.
22. Link TM, Berning W, Scherf S, et al. CT of metal implants: reduction of artifacts using an extended CT scale technique. J Comput Assist Tomogr. 2000;24:165–72.
23. Meyer E, Raupach R, Lell M, Schmidt B, Kachelriess M. Normalized metal artifact reduction (NMAR) in computed tomography. Med Phys. 2010;37:5482–93.
24. Lemmens C, Faul D, Nuyts J. Suppression of metal artifacts in CT using a reconstruction procedure that combines MAP and projection completion. IEEE Trans Med Imaging. 2009;28:250–60.
25. Yu L, Li H, Mueller J, et al. Metal artifact reduction from reformatted projections for hip prostheses in multislice helical computed tomography techniques and initial clinical results. Investig Radiol. 2009;44:691–6.
26. Prell D, Kyriakou Y, Kachelrie M, Kalender WA. Reducing metal artifacts in computed tomography caused by hip endoprostheses using a physics-based approach. Investig Radiol. 2010;45:747–54.

27. Coupal TM, Mallinson PI, McLaughlin P, Nicolaou S, Munk PL, Ouellette H. Peering through the glare: using dual-energy CT to overcome the problem of metal artefacts in bone radiology. Skelet Radiol. 2014;43:567–75.
28. Stolzmann P, Winklhofer S, Schwendener N, et al. Mono-energetic computed tomography reconstructions reduce beam hardening artifacts from dental restorations. Forensic Sci Med Pathol. 2013;9:327–32.
29. Stolzmann P, Leschka S, Scheffel H, et al. Characterization of urinary stones with dual-energy CT: improved differentiation using a tin filter. Investig Radiol. 2010;45:1–6.
30. Bamberg F, Dierks A, Nikolaou K, Reiser MF, Becker CR, Johnson TR. Metal artifact reduction by dual energy computed tomography using monoenergetic extrapolation. Eur Radiol. 2011;21:1424–9.
31. Zhou C, Zhao YE, Luo S, et al. Monoenergetic imaging of dual-energy CT reduces artifacts from implanted metal orthopedic devices in patients with factures. Acad Radiol. 2011;18:1252–7.
32. Meinel FG, Bischoff B, Zhang Q, Bamberg F, Reiser MF, Johnson TR. Metal artifact reduction by dual energy computed tomography using energetic extrapolation: a systematically optimized protocol. Investig Radiol. 2012;47:406–14.
33. Landis JR, Koch GG. The measurement of observer agreement for categorical data. Biometrics. 1977;33:159–74.
34. Meyers CR, Blesh TE. Measurement in physical education. New York: Ronald Press; 1962.
35. Guggenberger R, Winklhofer S, Osterhoff G, et al. Metallic artifact reduction with mono-energetic dual-energy CT: systematic ex vivo evaluation of posterior spinal fusion implants from various vendors and different spine levels. Eur Radiol. 2012;22:2357–64.
36. White LM, Buckwalter KA. Technical considerations: CT and MR imaging in the postoperative orthopedic patient. Semin Musculoskelet Radiol. 1977;6:5–17.